ELSEVIER

Thermochimica Acta 376 (2001) 147–154

thermochimica acta

www.elsevier.com/locate/tca

Thermodynamic studies of solids with non-negligible vapour pressure: *T–v* and *p–T* diagrams of the dimorphism of adamantane

P. Espeau*, R. Céolin

Laboratoire de Chimie Physique, Faculté des Sciences Pharmaceutiques et Biologiques, Université Paris 5, 4 avenue de l'Observatoire, F-75006 Paris, France

Received 9 February 2001; received in revised form 8 May 2001; accepted 8 May 2001

Abstract

A differential scanning calorimetry method, designed to determine the melting enthalpy of compounds with non-negligible vapour pressure, is applied to adamantane. This method is based upon the linear dependence of the melting-related thermal effect with the specific volume, i.e. the thermodynamic variable *v* considered for heterogeneous matter. This variable, regarded as the ratio between the inner volume of the DSC pan and the initial mass of solid sample, is used to construct *T–v* diagrams through which melting enthalpies at the triple point conditions are obtained.

A *T–v* diagram for adamantane is presented and $\Delta_{fus}H$ of $+(12.4 \pm 0.3)$ kJ mol^{-1} at $T_{fus} = 543 \pm 2$ K was found for this compound. The specific volume of the vapour phase was extrapolated to 52.7 ± 1.5 cm^3 g^{-1} at triple point conditions. With this information, a more general description of the *p–T* diagram for adamantane is put forward.

Keywords: Adamantane; *T–v* phase diagram; *p–T* phase diagram; Vapour pressure; Differential scanning calorimetry; Enthalpy of fusion

1. Introduction

Measurements of heats of fusion ($\Delta_{fus}H$) by means of differential scanning calorimetry (DSC) or differential thermal analysis (DTA) have nowadays become routine operations which do not apply to solids with non-negligible vapour pressure because sublimation occurs first, at least partially. This endothermally shifts the base line before the melting peak appears and prevents the mass of melting solid to be known. Attempts to bypass these sublimation-related effects are mostly carried out by enclosing solid samples inside hermetically sealed pans or tubes, strong enough to resist sublimation-induced pressure effects. Nevertheless, the acquisition of reliable results is hampered by the unavoidable existence of dead volumes inside the sample containers because mass losses due to sublimation are not suppressed even if they are reduced. Thus, data on melting for compounds with non-negligible vapour pressure are scarce or questionable.

This paper describes how a method designed to determine the enthalpy of fusion of arsenic [1] has been applied to adamantane for which enthalpies of fusion of either $+(13.958 \pm 0.279)$ [2] or

* Corresponding author. Tel.: +33-1-53-73-96-74; fax: +33-1-43-29-05-92.
E-mail address: espeau@pharmacie.univ-paris5.fr (P. Espeau).

0040-6031/01/$ – see front matter
PII: S0040-6031(01)00561-5

$+(12.80 \pm 0.04)$ [3], or even $+(8.0 \pm 0.4)$ kJ mol^{-1} [4] have been previously quoted and for which melting temperatures as disparate as 541 [5], 543.20 [2] and 552 K [4] have been reported. *T–v* and *p–T* diagrams of state for adamantane are also proposed based on the results presented here and on data gathered from the literature.

2. Method

2.1. General background

The existence of the solid, liquid and vapour states of a pure substance can be represented by surfaces in the *p–v–T* space. Among the three possible projections of these surfaces, only two are currently encountered: the projection on plane *p–v* and the projection on plane *p–T*. The third one, the projection on plane *T–v*, is seldom used, although it is the one which best accounts for interpreting DSC or DTA experiments on substances with non-negligible vapour pressures, as shown below.

The *T–v* projection in Fig. 1A shows how the single-phase regions are connected by two-phase regions and converge to the three-phase region. The latter, which corresponds to a point in plane *p–T* — the triple point — has thus, become a horizontal segment in plane *T–v*. This segment is defined by the same temperature as that of the triple point and by the specific volumes v_S (point A), v_V (point B) and v_L (point E) of the coexisting solid, vapour and liquid phases, respectively. The specific volume v_L lies generally between v_S and v_V, and closer to v_S than to v_V, because the volume change which occurs upon melting is small when compared to that which occurs upon sublimation or ebullition. It is worth noting that any point of this segment corresponds to a mixture of solid, liquid and vapour phases whose proportions depend on the *v* value for the mixture.

The *T–v* diagram in Fig. 1A also summarises the phase-change reactions that occur in a one-component system on heating any mass enclosed in any volume under equilibrium conditions. It follows that segment A–E–B corresponds to the reversible equilibrium which can be symbolised by

solid + vapour ⇔ liquid

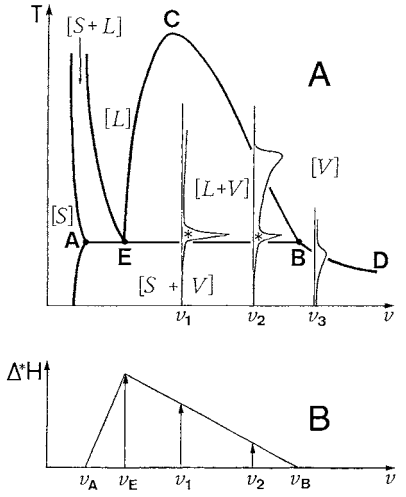

Fig. 1. (A) Schematic *T–v* diagram of a one-component system. The phase regions are identified by the symbols in brackets (S: solid, L: liquid, V: vapour). The A–E–B segment corresponds to the invariant equilibrium between solid, A; liquid, E; and vapour, B phases. Point C is the critical point of the liquid–vapour equilibrium. Three theoretical DSC curves exhibit the thermal effects expected on heating samples defined by v_1, v_2 and v_3 values ($v_i = V/m_i$, V = inner volume of the DSC pans, m_i = initial sample mass). (B) Tammann curve associated with the A–E–B segment. The reported ΔH values correspond to the areas of the starred peaks in Fig. 1A. Such peaks are not observed for $v_i > v_B$ because this condition implies the crossing of the B–D curve in Fig. 1A.

when the temperature increases and provided $v_L > v_S$ upon melting (it should be written as "solid ⇔ liquid +vapour", when *T* increases and $v_L < v_S$ instead upon melting, as it does for ice). According to the Le Chatelier's principle, both equilibria shift endothermally on heating.

The *T–v* diagram in Fig. 1A is thus, similar to that of a (solid + liquid 1 ⇔ liquid 2) monotectic equilibrium in the isobaric *T–x* representation of binary systems because in both cases there is a critical point at the upper limit of one of the two-phase regions above the invariant line. A Tammann curve is associated with such invariant equilibria. This curve, on which endothermic monotectic-related effects are plotted against molar fraction *x*, reaches a maximum at the molar fraction of the "liquid 2" monotectic liquid. Similarly, a Tammann curve can be associated with the A–E–B "triple segment", as shown in Fig. 1B. Heat $\Delta^* H$ associated with the endothermic shift of the invariant equilibrium is determined from

the area of DSC peaks like those starred in Fig. 1A. It varies as a function of the specific volume of analysed matter and reaches a maximum when liquid only (and not mixtures of liquid and solid or liquid and vapour phases) is formed on heating a (solid + vapour) mixture. This occurs when the specific volume of this mixture is the same as that of the liquid phase at the triple point.

2.2. Consequences

These considerations can be related to the thermal effects that take place when performing a DSC or DTA experiment on a solid phase with non-negligible vapour pressure. The solid is weighed and enclosed in a sealed pan: a dead volume remains which depends on the initial amount of solid, m, and on the inner volume of the pan, V. Assuming $V =$ constant over the experimental range of temperature (this may be approximated by using a pan made of a material with low or negligible thermal expansion, such as stainless steel or silica), and the pan strong enough to resist pressure, it follows that the mass of solid decreases as T increases due to sublimation although no matter is lost by effusion. If the amount of heat required to melt the residual solid is referred to the initial mass of sample, then the enthalpy of fusion is determined smaller than it should be. This happens when computer software used to calculate heats from DSC records take into account just the initial mass of sample.

This misfit can be avoided by considering the ratio $V/m = v$, i.e. the specific volume for heterogeneous matter, according to Gibbs [6]. Then, the melting enthalpy can be extrapolated through the Tammann curve to v_L (i.e. the v value for point E in Fig. 1B) because V/m is easily varied by changing either m or V. In other words, the Tammann curve for the E–B section of the ''triple segment'' concerning melting can be drawn from DSC data. As a matter of fact, three types of DSC curves are shown in Fig. 1A. The heats related to the (starred) endothermic peaks on the theoretical DSC curves for v_1 and v_2 are reported on the Tammann curve in Fig. 1B as a function of $v = V/m$. When v_E is known, the corresponding melting enthalpy may be determined by extrapolating from experimental data obtained for the $v_E < v < v_B$ range. The same applies to v_B which corresponds to the specific volume of the vapour phase at triple point conditions. The DSC curve obtained for v_3 is observed when V/m is high enough so that no solid remains when the melting temperature is reached. The peak maximum on this curve indicates that the solid–vapour equilibrium no longer exists in the sample container. Its temperature corresponds to a point on curve BD, the border between [solid + vapour] and [vapour] phase regions in the T–v diagram, which can then be partially drawn.

3. Experimental

Adamantane (tricyclo[3.3.1.1^{3,7}]decane), $C_{10}H_{16}$, was purchased from Janssen (purity $> 99\%$) and sublimed before use. At ordinary pressure, tetragonal SII adamantane is the stable phase at low temperatures (space group $P\text{-}42_1c$, $a = 6.641$ Å and $c = 8.875$ Å at 208.6 K [7], $a = 6.60$ Å and $c = 8.81$ Å at 163 K [8] and $a = 6.639$ Å and $c = 8.918$ Å at 188 K [9]). It transforms into a cubic S_I plastic phase at 208.55 K [10]. The latter (space group $Fm3m$, $a = 9.42$ [5], 9.445 [8,11], 9.43 [12] or 9.426 Å [13] at 293 K) melts at 541 [5], 542 [14] or 552 K [4].

DSC experiments were performed with a TA 2000 thermal analyser (TA Instruments) and a Perkin-Elmer DSC-7 apparatus at a scanning rate of 5 K min^{-1}. The apparatuses were calibrated with Indium, the current standard for the determination of enthalpy changes and phase transition temperatures. Setaram and Perkin-Elmer high-pressure steel crucibles (30 μl inner volume) were filled with masses of adamantane ranging between 0.67 and 26.97 mg. They were weighed with microbalances sensitive to 0.01 mg.

4. Results and discussion

4.1. Adamantane T–v diagram

Three types of DSC curves (Fig. 2) similar to those shown in Fig. 1A were obtained for adamantane as a function of the V/m ratio.

1. With low V/m values, DSC curves like curve A in Fig. 2 are recorded. They correspond to the thermal effect associated with crossing, on heating,

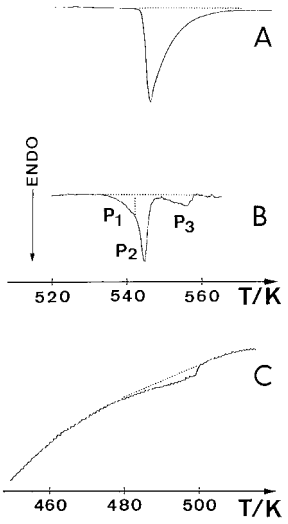

Fig. 2. Various types of DSC curves recorded for $v = V/m = 2.53$ (A), 42.9 (B) and 125 (C) $cm^3\ g^{-1}$. The endothermic effects are delimited by dotted lines.

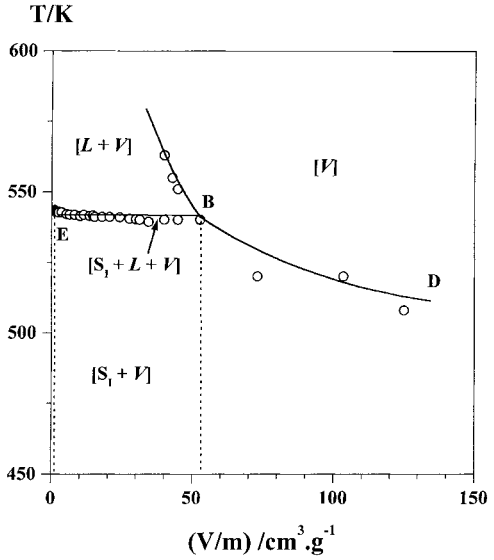

Fig. 3. T–v diagram of adamantane plotted from the experimental DSC results.

the E–B segment of the T–v diagram in Fig. 1A, and the onset temperature of the endothermic peak corresponds to the triple point temperature. This indicates that a (solid + vapour) mixture has transformed into a (liquid + vapour) mixture in the DSC pan.

2. DSC curves like curve B in Fig. 2 are obtained from samples with V/m values high enough for curve BC in Fig. 1A to be reached on heating. In the DSC pan, a (solid + vapour) mixture becomes a (liquid + vapour) mixture (at the onset temperature of part P_2 of the first peak), which in turn transforms into the vapour phase (at the temperature of the maximum of the broad peak P_3). The melting-related P_2 effect is preceded by a pre-signal P_1 due to sublimation. Then, integration of the first peak ($P_1 + P_2$) would lead to an enthalpy value that would encompass a sublimation effect. The latter was skirted by doing no integration for $V/m \geq 35\ cm^3\ g^{-1}$, value up to which no pre-peak was observed.
3. With high V/m values, DSC curves like curve C in Fig. 2 are recorded. They show that the initial solid sublimes in the DSC pan without melting and that this process ends at the temperature of the maximum (T_{max}) of the endothermic peak. Thus, part of curve BD of the T–v diagram in Fig. 1A can be drawn by plotting T_{max} as a function of V/m (or v).

Results from 27 DSC experiments are compiled on the T–v diagram in Fig. 3. The temperatures for the experimental points that correspond to the E–B segment are computer-calculated at the onset of the melting peaks related to the sample fractions that have not sublimed. It is observed that the apparent melting temperature slightly decreases as v increases. This is due to partial sublimation that endothermally shifts the base line and that decreases the slope of the melting-related peak as v increases. As a consequence, the greater the sublimation, the lower the computer-calculated melting temperature. This is why the triple point temperature was extrapolated to $v = 0$ as being 543 ± 2 K, i.e. a value closer to 541 K [5] than to 552 K [4], using just the T_{fus} values for $v < 35\ cm^3\ g^{-1}$.

The Tammann curve in Fig. 4 corresponds to the thermal effects related to the E–B segment in Fig. 3. They were determined from the areas of peaks like the one in Fig. 2A (or like starred peaks in Fig. 1A). The curve was least-squares refined assuming a linear relationship between Δ^*H values (in $J\ g^{-1}$) and V/m values (in $cm^3\ g^{-1}$), and the result was:

$$\Delta^*H = -1.765 \times \frac{V}{m} + 93.080 \quad (r^2 = 0.994) \qquad (1)$$

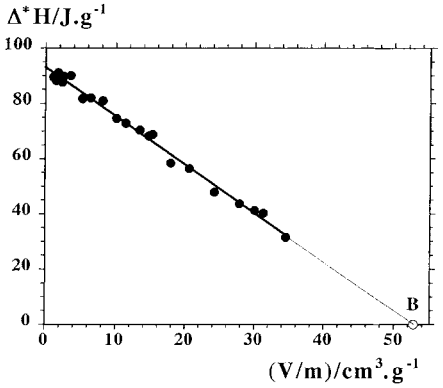

Fig. 4. Tammann curve related to the E–B segment in Fig. 3. The Δ^*H values were obtained exclusively from peaks like the one in Fig. 2A, i.e. with no pre-peak P_1 (see Fig. 2B).

The specific volume (v_V) of the saturating vapour phase at the melting temperature corresponds to the *V/m* value for point B. From Eq. (1), it was found to be 52.7 $cm^3\ g^{-1}$ with an uncertainty of about 3% graphically determined from Fig. 4. This value led to a molar weight of 150.54 g mol^{-1} (instead of 136.24 g mol^{-1}) assuming that adamantane vapour behaves as a perfect gas and resorting to the pressure at the triple point found to be 569048 Pa (*vide infra*). Its compression factor ($Z = 0.905$) indicates that adamantane vapour at the triple point behaves as a real gas ($Z < 1$) at intermediate pressures.

The melting enthalpy, $\Delta_{fus}H$, may be now determined from the Δ^*H value at v_E since it corresponds to the maximum of the Tammann curve concerning the solid + vapour ⇔ liquid equilibrium, i.e. segment A–B in Fig. 1B.

No data were obtained for the A–E section of this segment because if T_{fus} were reached no dead volume would remain in the DSC pans when $V/m < v_E$, and pressure would become huge. Nevertheless, *V/m* values for points A and E, which correspond to the specific volumes of the solid and liquid phases in equilibrium with the vapour phase at the (solid + liquid + vapour) triple point, may be estimated as follows.

The unit-cell volumes of the S_{II} and S_I phases have been determined by Amoureux and Foulon [9] in the 122–208.6 and 208.6–294 K range, respectively. From this work, it can be found that both molecular volumes linearly vary with temperature ($V(S_{II})$ $(Å^3) = 188.99 + 0.040365 \times T$ (K) $(r^2 = 0.993)$ and $V(S_I)$ $(Å^3) = 187.73 + 0.075076 \times T$ (K) $(r^2 = 0.983)$). Thus, the specific volume of the fcc plastic phase is estimated at $v(S_I) = v_A = 137.6\ cm^3\ mol^{-1}$ $(1.010\ cm^3\ g^{-1})$ at 543 K, assuming that it linearly varies from 294 up to 543 K.

Taking into account that the volume change at the melting point is 0.046 $cm^3\ g^{-1}$ (6.267 $cm^3\ mol^{-1}$) [3], the specific volume of the liquid is then $v_L = 1.056\ cm^3\ g^{-1}$ (143.9 $cm^3\ mol^{-1}$). This is the value for point E in Fig. 1 which corresponds to the maximum of the Tammann curve. Using Eq. (1), the melting enthalpy, $\Delta_{fus}H$, is calculated to be +91.20 J g^{-1} (+12.43 kJ mol^{-1}). This closely agrees with one of the values (+12.8 kJ mol^{-1}) [3] previously found and disagrees with the +8 kJ mol^{-1} value [4], which might thus, correspond to experiments performed with $V/m = 20\ cm^3\ g^{-1}$. If an extrapolation were performed to $v = 0$, the melting enthalpy would be +12.68 kJ mol^{-1}. Bearing in mind that data from DSC measurements are currently affected by an error of about 5%, the result would fall within the experimental uncertainty.

4.2. Adamantane p–T diagram

This value ($\Delta_{fus}H = +12.43$ kJ mol^{-1}) was used for constructing an improved description of the adamantane *p–T* diagram. Since two polymorphs (S_I and S_{II}) of adamantane are known, four invariant equilibria (or triple points) are to be located in the *p–T* diagram: namely S_I–L–V, S_{II}–L–V, S_I–S_{II}–L and S_I–S_{II}–V. Each of them is located at the crossing point of three out of six two-phase equilibrium curves bordering the single-phase regions, as shown on the topological representation in Fig. 5.

4.2.1. Triple point S_I–L–V

The $p = f(T)$ curve for equilibrium S_I–L was studied up to 25 kbar and was fitted to the Simon equation by Pistorius and Resing [3]. They found:

$$p(\text{kbar}) = 2.392 \times \left[\left(\frac{T(\text{K})}{541}\right)^{8.493} - 1\right] \quad (2)$$

assuming $T_{fus} = 541$ K at "zero" pressure. This allowed these authors to estimate the initial slope of the melting curve at $dT/dp = 26.6 \pm 4$ K $kbar^{-1}$.

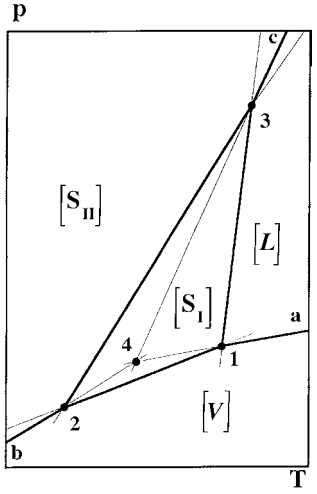

Fig. 5. Schematic p–T diagram of adamantane showing its dimorphism and the relative location of the four triple points that ensue: $1 = S_I{-}L{-}V$, $2 = S_I{-}S_{II}{-}V$, $3 = S_I{-}S_{II}{-}L$ and $4 = S_{II}{-}L{-}V$ (metastable).

However, the pressure value for this triple point is not zero, but that of the saturating vapour under which melting occurs. This value can be calculated at $T = 543$ K, by equalising the equations for the S_I–V and L–V equilibrium curves.

Recommended vapour pressures for the S_I–V equilibrium in the 223–33 K range [15] were fitted to the following equation:

$$p(\mathrm{Pa}) = 20.054 \times 10^{10} \times \mathrm{e}^{-6935.5/T(\mathrm{K})} \quad (r^2 = 0.997) \tag{3}$$

in which number 6935.5 is the ratio between the sublimation enthalpy $\Delta_{sub}H$ and the gas constant R. This leads to an enthalpy of sublimation of $+57.66$ kJ mol^{-1} and to a calculated vapour pressure of 569048 Pa at triple point S_I–L–V ($T = 543$ K). Then an enthalpy of vaporisation $\Delta_{vap}H = +45.23$ kJ mol^{-1} is obtained at 543 K according to $\Delta_{sub}H(S_I) = \Delta_{fus}H + \Delta_{vap}H$, taking $\Delta_{fus}H = +12.43$ kJ mol^{-1} (this work) and $\Delta_{sub}H(S_I) = +57.66$ kJ mol^{-1}.

Assuming that the L–V equilibrium curve, which meets both S_I–V and S_I–L curves at the S_I–L–V triple point, may be described by an equation of the type of Eq. (3), and using $p = 569048 = a \times 10^{11} \times \mathrm{e}^{b/543}$ and $b = -45230/8.314 = -5440.2$, it follows that the $p = f(T)$ equation for equilibrium L–V is

$$p(\mathrm{Pa}) = 1.277 \times 10^{10} \times \mathrm{e}^{-5440.2/T(\mathrm{K})} \tag{4}$$

4.2.2. Triple point S_I–S_{II}–L

Phase-changes of crystalline adamantane under pressure were studied by Pistorius, Snyman and Resing [3,16] and by Hara et al. [17]. The former authors found that the co-ordinates for triple point S_I–S_{II}–L are $p = 27$ kbar and $T = 743$ K and that the dp/dT slope for the S_I–S_{II} equilibrium curve equalled $51(\pm 4)$ bar K^{-1}. This line may thus, be described by

$$p(\mathrm{Pa}) = (51 \times 10^5 \times T(\mathrm{K})) - 1.064 \times 10^9 \tag{5}$$

assuming that it goes through the (27 kbar, 743 K) triple point and the S_I–S_{II} transition point which occurs at 208.6 K when no pressure is applied. It is worth noting that Eq. (2) used by Pistorius and Resing [3] to describe the S_I–L equilibrium curve equals Eq. (5) for p–T values lower than those they proposed for the S_I–S_{II}–L triple point. Since the experimental points for the S_I–L equilibrium in the 631–710 K range can be fitted to

$$p(\mathrm{Pa}) = 194.64 \times 10^5 \times T(\mathrm{K}) - 11.752 \times 10^9 \quad (r^2 = 0.989) \tag{6}$$

the values $p = 27.3 \times 10^8$ Pa and $T = 744$ K for the S_I–S_{II}–L triple point co-ordinates are extrapolated by equalising Eqs. (5) and (6).

Pistorius and Snyman [16] also estimated that the heat of transition from S_{II} to S_I, $\Delta_{trans}H(S_{II} \rightarrow S_I)$, is about $+2.75$ kJ mol^{-1}. This falls in the vicinity of the experimental value (3.376 ± 0.010 kJ mol^{-1}) found by Chang and Westrum [10].

4.2.3. Triple point S_I–S_{II}–V

The S_I–S_{II}–V triple point is located at the crossing point ($T = 208.6$ K) of curves S_I–V, S_{II}–V and S_I–S_{II}. Since pressure is assumed to be the same for S_I–V and S_{II}–V equilibria at the triple point temperature, the pressure at 208.6 K may be calculated from Eq. (3), giving $p = 7.29 \times 10^{-4}$ Pa.

4.2.4. Triple point S_{II}–L–V

The S_{II}–L–V triple point is metastable because it is located on the metastable extension of curve L–V at the crossing point of curves L–V and S_{II}–V.

The sublimation enthalpy for S_{II} may be determined from $\Delta_{sub}H(S_{II}) = \Delta_{sub}H(S_I) + \Delta_{trans}H(S_{II} \rightarrow S_I)$ as $\Delta_{sub}H(S_{II}) = +61.04$ kJ mol^{-1}.

Incorporating this value together with $p = 7.29 \times 10^{-4}$ Pa and $T = 208.6$ K in an equation of the $p = a\,e^{-\Delta H/RT}$ type, assumed to apply both to S_I–V and S_{II}–V curves, the equation for the S_{II}–V equilibrium becomes

$$p(\text{Pa}) = 14.033 \times 10^{11} \times e^{-7341.4/T(\text{K})} \quad (7)$$

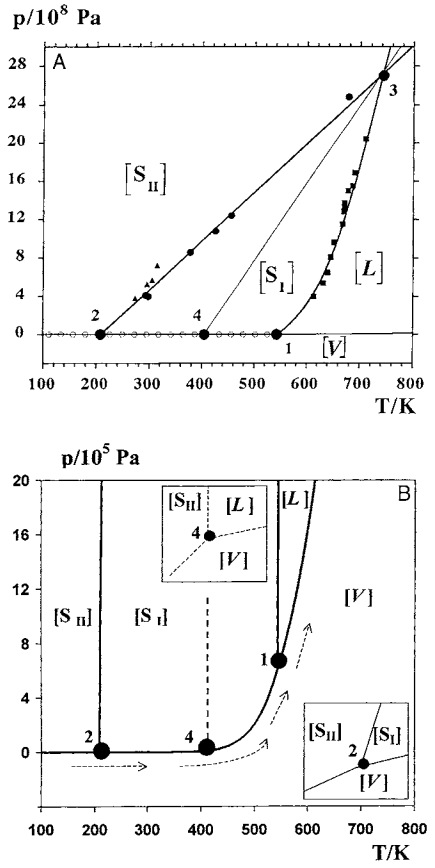

Fig. 6. *p–T* diagram of adamantane plotted from experimental data and using Eqs. (2)–(5) (see text). (A) High-pressure region, (B) low-pressure region. Experimental points: (■) from [3], (●) from [16], (▲) from [17] and (○) from [15]. The triple points and phase regions are identified as in Fig. 5. The dotted arrows in Fig. 6B indicate the path of least variance followed upon heating samples enclosed in sealed pans. Insets show how the two-phase equilibrium curves involving the vapour phase cross at invariant points 2 and 4.

Table 1
Round values for p and T at the four triple points that occur in the p–T diagram of adamantane because of its dimorphism

Triple point	p (Pa)	T (K)
S_I–L–V	60×10^4	543
S_I–S_{II}–L	27×10^8	744
S_I–S_{II}–V	73×10^{-5}	209
S_{II}–L–V	19×10^3	405

After equalising Eqs. (4) and (7), co-ordinates $p = 18.49 \times 10^3$ Pa and $T = 404.6$ K were calculated for triple point S_{II}–L–V.

Since triple points S_{II}–L–V and S_I–S_{II}–L are linked through curve S_{II}–L, an equation for the metastable part of this curve may be obtained assuming a linear relationship between p and T, and using $dp/dT = 8.04 \times 10^6$ Pa K^{-1} calculated from the co-ordinates of the two triple points. The following equation, thus, tentatively describes the S_{II}–L equilibrium curve:

$$p(\text{Pa}) = 8.04 \times 10^6 \times T(\text{K}) - 3.253 \times 10^9 \quad (8)$$

Fig. 6 is an overview of the *p–T* diagram of adamantane constructed from Eqs. (2)–(8) for stable and metastable monovariant equilibria. As can be seen, the calculated results agree rather well with the experimental data. Round p and T values for the four triple points have been compiled in Table 1.

5. Concluding remarks

To sum up, DSC measurements on compounds with non-negligible vapour pressure such as adamantane show that the area of the peak observed upon fusion depends on how the DSC pans are filled, which may lead to grossly inaccurate results and which might even explain the dearth of such data.

The method used in this work allows to skirt the drawbacks derived from the presence of a non-negligible vapour phase upon fusion. In addition, the *T–v* diagram of the substance in question may be at least partially drawn resorting to basic classic thermodynamics. According to the Tammann method, the thermal effect associated with the crossing of the fusion triple point may be referred to the thermodynamic variable v, taken as the V/m ratio between the sealed pan internal volume V and the constant mass m of a

sample placed inside it. This leads, upon extrapolation, to the fusion enthalpy value at the (solid+ liquid + vapour) triple point conditions.

In addition, these measurements restate that the path followed in the *p–T* diagram of a solid with non-negligible vapour pressure (such as arsenic [1] or adamantane) is a least-variance path (see arrows in Fig. 6B) when DSC runs are performed using sealed pans. This contradicts the widespread assumption that a path under constant atmospheric pressure is followed upon heating. However, DSC apparatuses are not sensitive enough for the vaporisation influence to be observed as it is, for instance, for adamantane, whose behaviour may be considered the normal one and not an exception. Indeed, even if the vapour pressure remains very low, it increases on heating.

Finally, it has also been shown how data from high-pressure experiments and vapour-pressure values may be combined to draw *T–v* and *p–T* diagrams for adamantane which are topologically related to the case of dimorphism usually exemplified by sulphur.

Acknowledgements

Professor J.Ll. Tamarit (Universitat Politecnica de Catalunya, Barcelona, Catalunya), Professor J. Jose (Université Claude Bernard, Lyon, France), and Dr. P. de Oliveira are kindly acknowledged for experimental assistance, pre-printed informations and language assistance, respectively.

References

[1] J.-C. Rouland, R. Céolin, C. Souleau, P. Khodadad, J. Thermal Anal. 23 (1982) 143.
[2] G.J. Kabo, A.V. Blokhin, M.B. Charapennikau, A.G. Kabo, V.M. Sevruk, Thermochim. Acta 345 (2000) 125.
[3] C.W.F.T. Pistorius, G.C. Resing, Mol. Cryst. Liq. Cryst. 5 (1969) 353.
[4] Z.-Y. Zhang, M. Frenkel, K.N. Marsh, R.C. Wilhoit, in: K.N. Marsh (Ed.), Landolt–Börnstein. Numerical Data and Functional Relationships in Science and Technology, New series, Group IV: Macroscopic Properties of Matter, Vol. 8: Thermodynamic Properties of Organic Compounds and their Mixtures, Subvol. A: Enthalpies of Fusion and Transition of Organic Compounds, Springer, Berlin, 1995, p. 252.
[5] E.Yu. Tonkov, High Pressure Phase Transformations: Handbook, Vol. 1, Gordon and Breach, Philadelphia, 1992, p. 156.
[6] J.W. Gibbs, The Scientific Papers of Thermodynamics, Dover, New York, 1961, p. 3.
[7] K.V. Mirskaya, Kristallografiya 8 (1963) 225.
[8] C.E. Nordmann, D.L. Smitkons, Acta Cryst. 18 (1965) 764.
[9] J.P. Amoureux, M. Foulon, Acta Cryst. B43 (1987) 470.
[10] S.S. Chang, E.F. Westrum Jr, J. Phys. Chem. 64 (1960) 1547.
[11] J.P. Amoureux, M. Bee, J.C. Damien, Acta Cryst. B36 (1980) 2633.
[12] W. Nowacki, Helv. Chim. Acta 28 (1945) 1233.
[13] A.I. Kitaigorodskii, Organic Chemical Crystallography, Consultant Bureau, New York, 1961, p. 333.
[14] S. Landa, S. Kriebel, E. Knobloch, Chem. Listy 48 (1954) 161.
[15] I. Mokbel, K. Rúzicka, V. Majer, V. Rúzicka, M. Ribeiro, J. Jose, M. Zábransky, Fluid Phase Equilibria 169 (2000) 191.
[16] C.W.F.T. Pistorius, H.C. Snyman, J. Phys. Chem. 43 (1964) 278.
[17] K. Hara, Y. Katou, J. Osugi, Bull. Chem. Soc. Jpn. 54 (1981) 687.